JOURNAL OF MATERIALS SCIENCE 15 (1980) 601–610

Compressive creep of Si_3N_4/MgO alloys

Part 1 *Effect of composition*

F. F. LANGE, B. I. DAVIS, D. R. CLARKE
Rockwell International Science Center, Thousand Oaks, California 91360, USA

The compressive creep behaviour of four compositions within the Si_3N_4–Mg_2SiO_4–Si_2N_2O compatibility triangle were studied in air at 1400° C. Strain rate ($\dot{\epsilon}$) versus stress (σ) was analysed to determine the stress exponent, n ($\dot{\epsilon} = A\sigma^n$). Cavitation during creep was determined by precise (sink–float) density measurements. Compositions close to the Si_3N_4–Si_2N_2O tie line exhibited no cavitation and had $n \simeq 1$, whereas compositions close to the Si_3N_4–Mg_2SiO_4 tie line exhibited extensive cavitation and had $n \simeq 2$. Test results are interpreted in terms of the volume fraction of the viscous phase present.

1. Introduction

Composition strongly affects the creep resistance of polyphase Si_3N_4 alloys fabricated with a densification aid [1–8]. Investigators who have examined the creep resistances of a variety of Si_3N_4 alloys have shown that the creep rate at a specific temperature and stress can vary by orders of magnitude depending on composition [1, 2]. The effects of some impurities [8] (e.g. CaO) and gross composition [1, 2, 5, 7] (type and amount of the densification aid) have been qualitatively documented.

Earlier investigators suggested that the general degradation of mechanical properties at high temperatures was due to the presence of viscous phase between the Si_3N_4 grains. High-resolution electron microscopy work has since confirmed that a continuous glassy phase does exist in most Si_3N_4 alloys [9, 10]. Assuming that the composition of the glassy phase is similar to the eutectic composition (i.e. the last liquid to solidify during cooling) of the compatibility triangle in which the composition was fabricated, Lange [11] pointed out that the content of the glass will depend on composition in the manner described by rules of phase equilibria; the volume fraction of the glassy "grain-boundary phase" will increase as the composition of the alloy is shifted toward the eutectic composition. Likewise, the temperature where degradation is first apparent should be related to the eutectic temperature. Since impurities must be included in phase equilibrium considerations, they will influence the eutectic composition and temperature. In this manner, the effects of impurities and gross composition can be combined, shifting the alloy composition either toward or away from the eutectic composition to either decrease or increase the high temperature properties, respectively [11]. The observed change in strength with composition for three series of materials in the Si–Mg–O–N system is consistent with this idea [12]. It is expected that creep resistance should follow suit.

Most investigators have directed the analysis of creep behaviour in terms of phenomena which produce cavities. This direction resulted from both TEM studies which reveal cavities at triple points in crept specimens [3, 4] and stress exponents for creep rate that do not correspond to conventional (e.g. diffusion and/or dislocation) models. One notable exception to this general trend was Seltzer's [2] observation of a linear stress dependence for several compositions in the Si–Al–O–N system fabricated with $\leqslant 30$ wt % Al_2O_3.* Other materials in this same system containing $\geqslant 40$ wt % Al_2O_3 had larger stress exponents, consistent with those reported for all other Si_3N_4 materials [2]. Thus, Seltzer's measurements suggest that at least two different mechanisms can dominate the creep

* This complete series of alloys, fabricated by the present author, were hot-pressed with 20, 30, 40 and 50 wt % Al_2O_3 plus Si_3N_4 [13].

0022–2461/80/030601–10$03.00/0

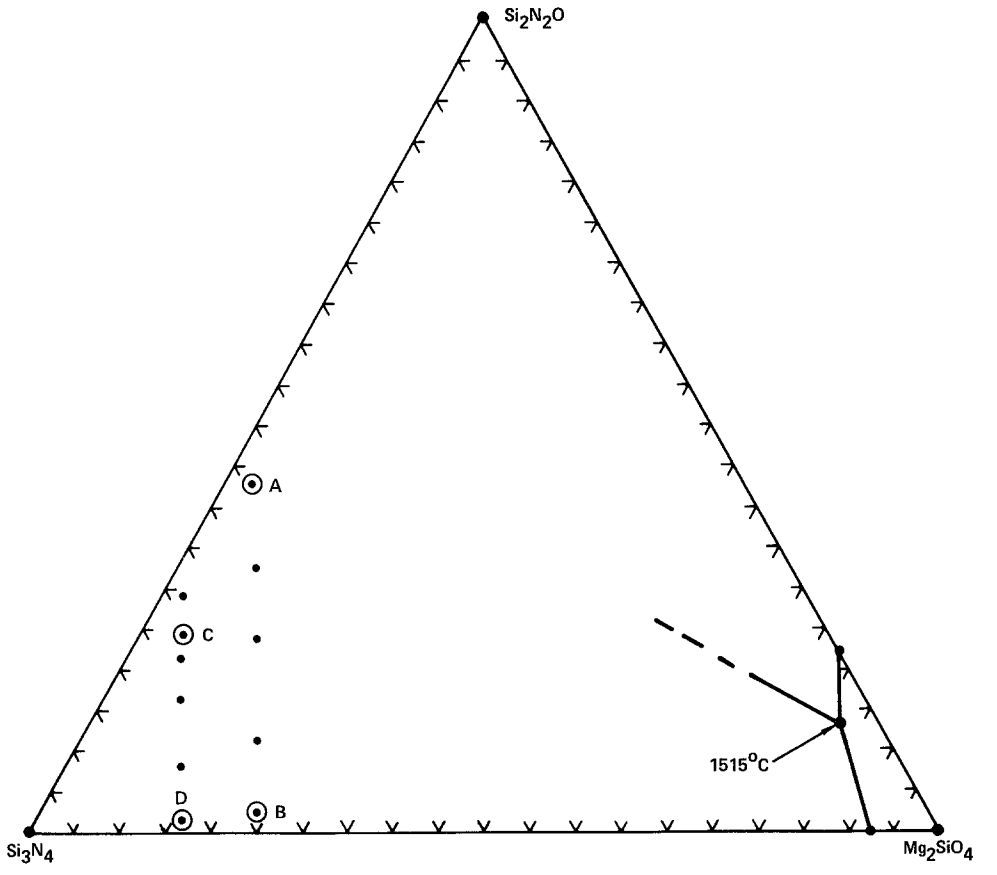

Figure 1 The Si_3N_4–Mg_2SiO_4–Si_2N_2O system illustrating compositions of materials used in this study in relation to eutectic composition.

behaviour of Si_3N_4 alloys, and a shift from one mechanism to another depends on composition.

The purpose of the present work was to characterize the creep behaviour of Si_3N_4 alloys as a function of composition in an attempt to classify the dominant creep mechanism in terms of the volume content of the glassy "grain-boundary phase". To accomplish this goal, well characterized alloy compositions were chosen from the Si_3N_4–Mg_2SiO_4–Si_2N_2O compatibility triangle of the Si–Mg–O–N system. Since eutectics in this compositional area are known, the relative volume fraction of the glassy phase for each composition could be estimated and related to the observed creep phenomena.

2. Experimental details

2.1. Materials

The compositions of the four materials (A, B, C, D) chosen for extensive study were part of two series of materials fabricated for a previous study concerning strength and oxidation [12]. Fig. 1 illustrates the compositions of these four materials (circled points), the compositions of the other materials within the two series, and the eutectic compositions and temperatures previously determined. All materials shown in Fig. 1 were prepared from high purity Si_3N_4 (e.g. 160 ppm Ca, 0.6 wt % O_2), SiO_2 and MgO powders, ball milled with WC media in plastic bottles, and hot-pressed at 1750° C for 2 h as reported elsewhere [12].

Phase identification was by X-ray diffraction. All materials contained β-Si_3N_4 and WC. Compositions A and C, contained Si_2N_2O in apparent proportion to that indicated by their position in the phase diagram; no Si_2N_2O was detected in B and D. The Mg_2SiO_4, expected to be present in all compositions, was not observed as a crystalline phase.

All materials were examined by transmission electron microscopy throughout this study. Dark-field imaging [14] revealed a glassy "grain-boundary phase" between all grains and at triple points as shown in Fig. 2. Extensive TEM work to

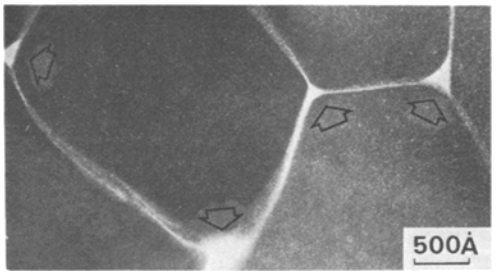

Figure 2 Dark-field image of the continuous glassy phase between Si_3N_4 grains.

quantify any difference in the volume content of the glassy phase in the four materials was not performed. Based on the above evidence (lack of a crystalline Mg_2SiO_4 phase and the presence of a glassy phase), the composition of the glassy phase was assumed to be the same as the ternary eutectic composition. Based on this assumption, the volume fraction of the glassy phase was estimated for each composition by using the lever rule to interpret the phase diagram and the appropriate molecular weights and densities.* Table I lists the estimated volume fractions of the glassy phase.

2.2. Creep experiments

Compressional creep testing was performed in air at 1400° C. Specimens (approximately 0.3 cm × 0.3 cm × 0.9 cm) were diamond cut and finished in a special jig so that parallelism of the two end surfaces was ensured. A high temperature extensiometer, described in the Appendix, was developed to measure strain. A dead weight, cantilevered (10:1) loading frame transmitted load to the specimen as shown in Fig. 10. The loading pads in contact with the specimen were made from either sintered or CVD SiC. Commercial grade, hot-pressed Si_3N_4 loading pads were observed to creep under the specimen and to result in unreliable strain measurements.

The apparent steady-state strain rates ($\dot{\epsilon}$) were analysed with respect to the empirical relation

$$\dot{\epsilon} = A\sigma^n \quad (1)$$

in an applied stress (σ) range between 70 and 700 MPa. Load was applied after the temperature was stabilized at 1400° C for a period of 1 h. Throughout each experiment, temperature did not vary more than ± 2° C. Because oxidation affects the creep behaviour of these materials (as detailed in Part 3 [15]), a new specimen was used at each stress; steady-state creep rates were determined for periods ⩽ 20 h. The total strain for any experiment never exceeded 0.05.

2.3. Density determinations

Because cavities were expected to form during creep, their volume content was determined by precise density measurements as a function of creep strain at a compressive stress of 350 MPa for materials C and D. To avoid the possible closure of cavities during cooling, the compressive load was not removed until the specimen was cool. Cavitation was also examined as a function of applied stress (175 to 700 MPa) with the same materials at a strain of 0.03. Density measurements were also performed on materials A and B, but only at a creep strain of 0.03 at 350 MPa.

A sink–float technique was developed to measure the volume fraction of cavities produced during creep. Mixtures of diiodemethane (ρ = 3.3 g cm^{-3}) and neothane (ρ = 1.3 g cm^{-3}) were prepared until the specimen would neither sink or float. To minimize the effect of volatilization, the liquid plus specimen were transferred to a pychnometer with a volume previously determined over a temperature range of 15 to 30° C. The pycnometer containing the liquid and specimen was then either heated or cooled slowly until the specimen was suspended within the liquid. Liquid was either removed or added to the pycnometer to compensate its volume change before weighing. With this technique, the density of a specimen could be

TABLE I Composition and phase content of creep specimens

Specimens	Composition (mole fraction)			Phases identified	Vol. fraction of glassy phase
	Si_3N_4	Si_2N_2O	Mg_2SiO_4		
A	0.54	0.43	0.03	β-Si_3N_4, Si_2N_2O, WC	0.04
B	0.74	0.03	0.23	β-Si_3N_4, WC	0.17
C	0.71	0.24	0.05	β-Si_3N_4, Si_2N_2O, WC	0.05
D	0.83	0.01	0.16	β-Si_3N_4, WC	0.11

* The density of the glass was assumed to be 3 g cm^{-3}.

reproduced by using different starting fluid mixtures to ± 0.0003 g cm^{-3}. That is, the technique was capable of reproducing a density measurement to ± 0.01%.

The density of each specimen was determined before and after the creep experiment. The oxide scale and material to the depth of ~ 0.02 cm below the scale/bulk interface was removed by surface grinding prior to measuring the density of the crept specimens. Several crept specimens with end cracks were diced into 2 or 3 pieces to preclude the effect of the crack. It was observed that the cracks did not significantly affect density. To preclude density changes that might arise through oxidation, differential densities of a series of specimens from materials C and D were determined as a function of oxidation period at 1400° C.

3. Results

3.1. General behaviour

The strain–time response of all stressed specimens included a small elastic deformation upon loading, a primary period in which the strain rate decreased with time and an apparent steady-state period. A final tertiary period, where the strain rate increased with time, was observed at higher stresses for materials B and D. Some of these specimens contained a small crack which propagated parallel to the loading direction. Upon unloading, all materials exhibited a small elastic recovery followed by an anelastic strain recovery; this is detailed in Part 2 [16].

The steady-state creep rate had to be defined in a somewhat arbitrary manner since a true steady-state condition was never observed. For tests where tertiary creep did not develop, the creep rate was always observed to slowly decrease with time. This decrease in strain rate was most pronounced for those materials that exhibited the greatest rate of oxidation (B and D). When a specimen was crept at successive stresses, the "steady-state" creep rate at the higher stress could be lower than that observed at the initial, lower stress. When the stress was then decreased back to the initial value and sufficient time was allowed for the anelastic recovery, the new "steady-state" creep rate was significantly smaller than the original value for the unstressed specimen.

After many frustrating and apparently inconsistent test results of this nature, it was hypothesized the creep resistance was improved by oxidation. The experiments and results detailing this phenomenon are reported in Part 3 [15]. Thus, in order to classify the materials examined with Equation 1, the steady-state creep rate was calculated from data taken over the last 4 h period of a test that was terminated after ~ 20 h. In this manner, the apparent steady-state creep rate for a new specimen of the same material could be reproduced within ± 15%. Steady-state values were not used if the specimen exhibited tertiary creep.

3.2. Strain-rate/stress response

Equation 1 was used in examining the apparent strain-rate/stress response of the four materials. Fig. 3 illustrates this representation of the data with a $\log \dot{\epsilon}$ versus $\log \sigma$ plot. As shown, composition strongly affects creep resistance. In

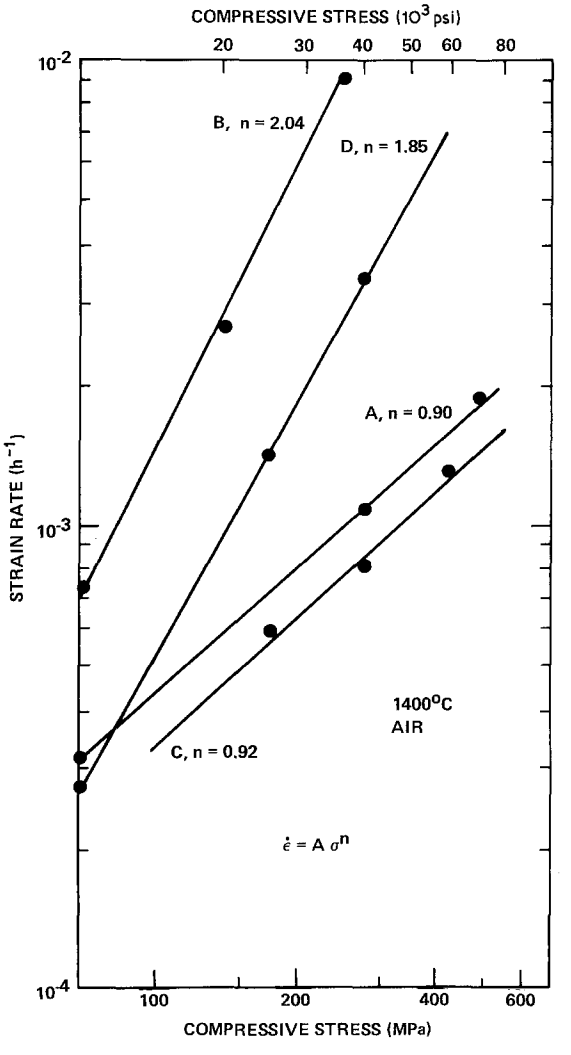

Figure 3 Apparent steady-state strain rate versus compressive stress of four materials examined; stress exponents (n) shown.

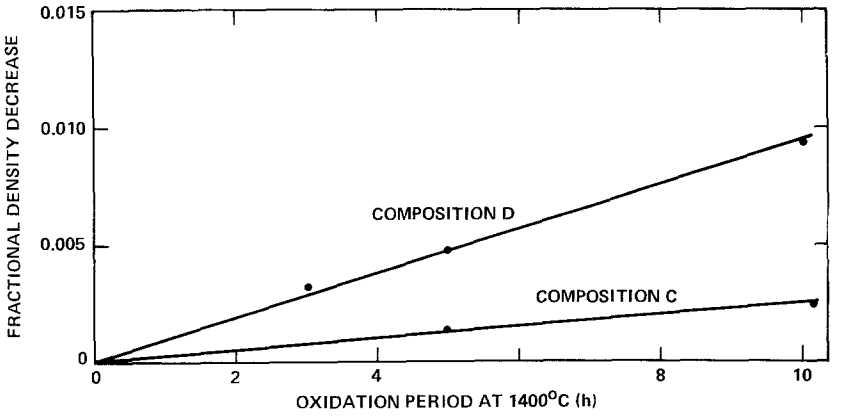

Figure 4 Fractional density change versus oxidation period at 1400° C for compositions C and D.

general, the material's resistance to creep can be ordered with respect to its estimated amount of glass phase (see Table I).

Strain-rate/stress exponents of materials closer to the ternary eutectic (B and D) are ~ 2, i.e. similar to values reported by others for commercial, hot-pressed material fabricated with MgO [2–5]. Stress exponents of materials furthermost from the ternary eutectic (A and C) are ~ 1. These data suggest that the principle mechanism responsibe for the creep behaviour strongly depends on composition.

3.3. Cavitation

Both cavitation and oxidation were found to affect density, therefore a control experiment was performed to determine the effect of oxidation alone on the change in density. The results for materials C and D are shown in Fig. 4. Compositional changes induced by oxidation are the cause of the observed decrease in density upon oxidation [17]; material D exhibited the greatest decrease because of its greater rate of oxidation.

The change in density (expressed as a void volume) observed for materials C and D as a function of creep strain is shown in Fig. 5. These data have been corrected for the density change induced by oxidation (Fig. 4). For material D, oxidation contributed between 20% and 30% of the total

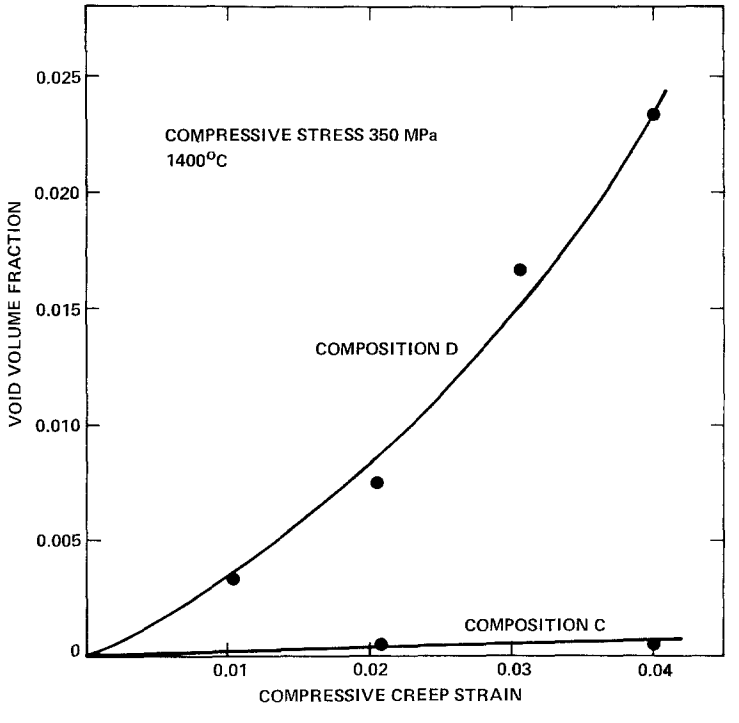

Figure 5 Fractional void volume versus creep strain under 350 Mpa compressive stress at 1400° C.

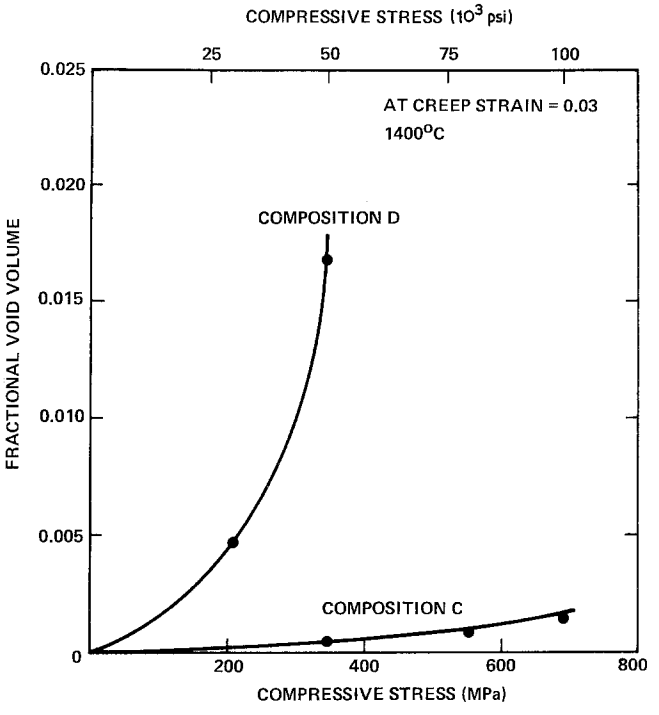

Figure 6 Fractional void volume versus compressive stress for strains = 0.03 at 1400° C.

density change. The effect of stress on the void volume produced at a creep strain of 0.03 is shown in Fig. 6. Results of single experiments with the other two materials showed that material B exhibited extensive cavitation, whereas material A exhibited negligible cavitation. TEM studies of the crept materials qualitatively showed that materials B and D contained a higher density of cavities relative to materials A and C, consistent with data shown in Figs. 5 and 6.

Since it was recognized that cavities can be produced during ion-milling of specimens prepared for TEM studies, precaution was extended in identifying cavities that were most likely produced by creep. These precautions included observing both uncrept and crept specimens of the same material and comparing cavities observed in both thick and thin portions of ion-milled foils. Wedge-shaped cavities, typified by the example shown in Fig. 7, made up the largest proportion of cavities observed in crept specimens. These cavities were observed at triple-point grain junctions. Their morphology (i.e. rounded corners) and the apparent amorphous nature of the material around the cavity boundary strongly suggest that these cavities were vapour bubbles that grew within the glass phase during creep. Although less frequently observed, cavities were also observed to form between two grains which separated in a direction normal to their common boundary as shown in Fig. 8a. The fibrilous nature of the apparent glassy phase between the separating grains is shown at higher magnification in Fig. 8b. Such fibrils are commonly observed in the tacky separation of printers' ink and are caused by the growth and linking of many small vapour bubbles. Fig. 8a also illustrates a large number of wedge-shaped cavities; the density of cavities in this portion of the specimen was somewhat higher than observed in other portions of the same foil.

It should be noted that the grains were relatively free of dislocations, suggesting that dislocation

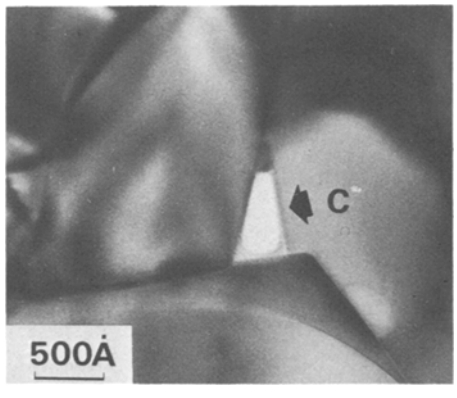

Figure 7 TEM micrograph of typical wedge-shaped cavity, C, produced during creep.

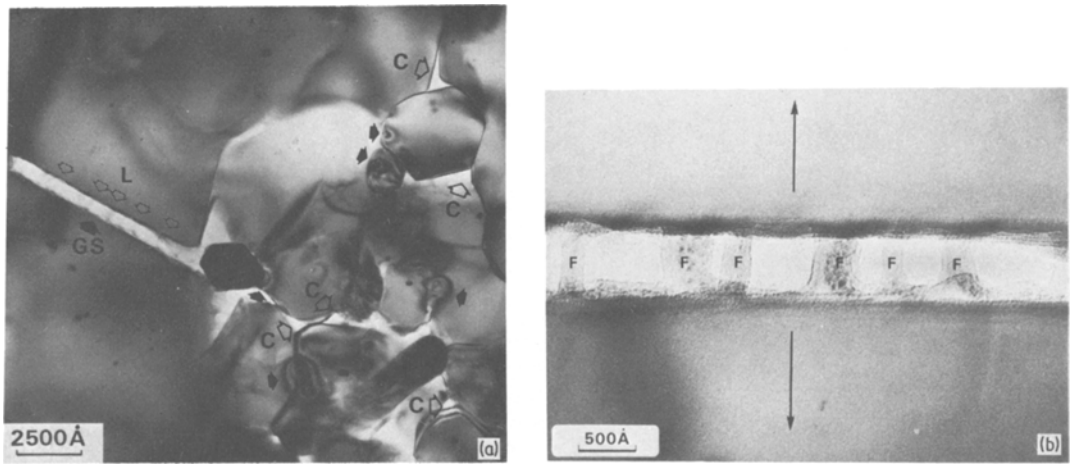

Figure 8 (a) Cavities produced by the separation of two grains perpendicular to their common boundary, (b) higher magnification of same grain pairs shows apparent glass fibrils, F.

motion is not a dominant mechanism of creep deformation in Si_3N_4 alloys up to temperatures of 1400° C. This same conclusion has also been reached by others [3, 4].

4. Discussion

The preceding experimental data clearly show that two concurrent mechanisms contribute to the creep behaviour of polyphase Si_3N_4 fabricated within the same compatibility triangle. Also, one mechanism can dominate the other depending on composition. The creep behaviour of compositions most remote from the ternary eutectic composition is dominated by an apparent diffusional mechanism which is indicated by both the linear stress dependence of the creep rate and the absence of cavitation. Cavitational creep is most pronounced in compositions closer to the ternary eutectic. For compositions in between those studied, it is presumed that the contribution of cavitation will decrease as the composition is shifted from one side of the compatibility triangle to the other. This hypothesis has been shown to occur, as detailed in a companion paper which discusses the effect of oxidation-induced compositional changes in creep behaviour [15].

The contribution of each of the two mechanisms to the general creep behaviour can be related to composition if it is assumed that both mechanisms are governed by the viscous, glassy phase and that the glassy phase has a composition close to that of the ternary eutectic composition. The latter assumption defines the volume fraction of glassy phase for any composition (see Section 2.1). The remainder of this section will relate the volume fraction of the viscous phase to the two mechanisms.

Diffusional creep in the context of the current Si_3N_4 alloys can be presumed to occur by the redistribution of matter through the viscous phase. Solution of Si_3N_4 and/or Si_2N_2O into the viscous phase and their reprecipitation elsewhere would be driven by differential chemical potentials that arise from localized stresses. The presence of localized stresses is documented in Part 2 which details the anelastic effect [16].

Stocker and Ashby [18] have modelled the diffusional creep of solid/liquid microstructures similar to that shown in Fig. 2. They assumed that the viscous grain-boundary phase "... enhanced creep by providing regions, or paths of high diffusive conductance" [18]. Differential chemical potentials that arise due to stress gradients provide the driving force for the diffusing species. Their analysis shows that the strain rate ($\dot{\epsilon}$) is related to the grain size (d), molar volume of the diffusing species (Ω), the molar fraction of the diffusing species (C) in the liquid, the volume fraction of the liquid phase (V_l),* the viscosity (η) of the liquid, and the applied stress (σ) as

$$\dot{\epsilon}_{\text{diff}} = \frac{8\Omega^{2/3}}{d^2\eta} CV_l\sigma. \qquad (2)$$

* Stocker and Ashby [18] assumed $V_l = S_0/d$, where S_0 is the thickness of the liquid phase between the grains. Lange [19] has shown that $V_l = 3S_0/d$; Equation 2 was thus modified by a factor of 3.

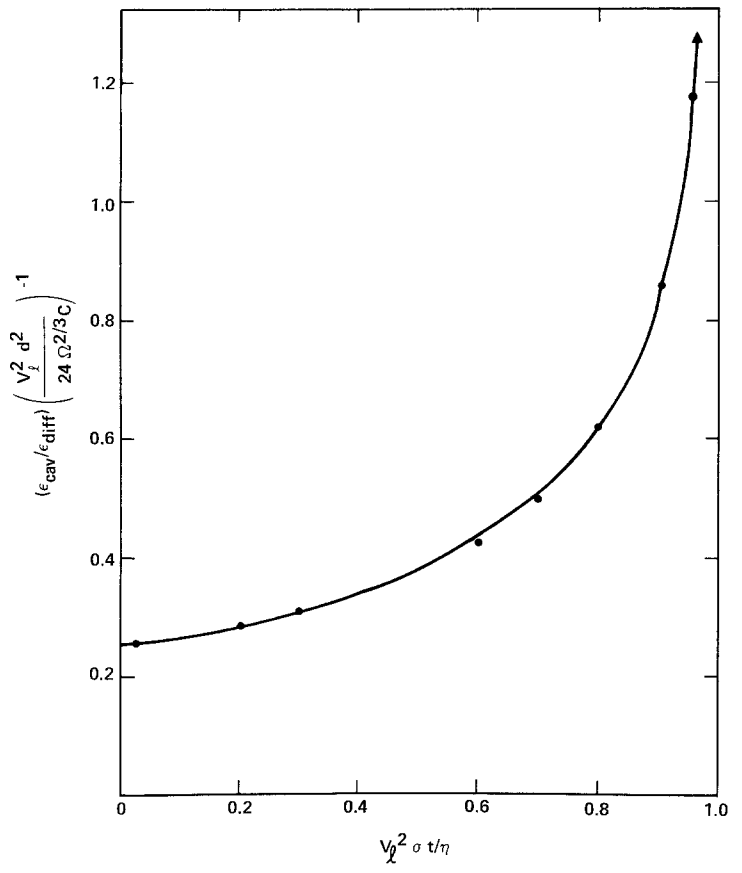

Figure 9 Comparison of strain produced by cavitation to strain produced by diffusion predicted for Equation 5.

Integrating this Equation assuming that the parameters on the RHS of Equation 2 are independent of time, results in

$$\epsilon_{diff} = \frac{8\Omega^{2/3} C V_l \sigma t}{d^2 \eta}, \qquad (3)$$

indicating the creep strain is linearly dependent on V_l, σ and time (t).

With regard to cavitational creep, most investigators suggest that grain-boundary sliding is required for the growth of cavities. Lange [19] has pointed out that cavitation requires the separation of grains. He showed that grain separation and not sliding is the rate-controlling step in the growth of cavities. The results of his analysis,

$$\epsilon_{cav} = \left[\left(1 - \frac{V_l^2 \sigma t}{\eta}\right)^{-1/4} - 1\right] \frac{V_l}{3}, \qquad (4)$$

indicates a relatively complex dependence on V_l, σ, and t and no direct dependence on grain size. It should be noted that the strain rate for cavitational creep as indicated by Equation 4 cannot be expressed as a simple power law with respect to either time or stress.

Although the analysis resulting in Equations 3 and 4 may not be sufficiently explicit to quantitatively predict creep strains, the equations can be used to predict trends. A comparison of Equations 3 and 4 can be made by dividing one by the other; after rearranging:

$$\frac{\epsilon_{cav}}{\epsilon_{diff}} \left(\frac{V_l^2 d^2}{24\Omega^{2/3} C}\right)^{-1} = \frac{(1 - V_l^2 \sigma t/\eta)^{-1/4} - 1}{V_l^2 \sigma t/\eta}. \qquad (5)$$

The LHS of Equation 5 is plotted as a function of the dimensionless product $V_l^2 \sigma t/\eta$ in Fig. 9 in order to examine the conditions where one mechanism may be more dominant than the other. As shown in Fig. 9, the contribution of cavitational creep increases with increasing $V_l^2 \sigma t/h$, i.e. larger volume fractions of the liquid, higher stresses, longer times and lower viscosity. Because V_l is squared, changes in V_l will have a greater effect than changes in the other factors. With other factors held constant, the contribution of cavitational creep will increase with increasing grain size.

The trends predicted by Equations 3 to 5 are consistent with experimental data:

(1) materials with large V_l cavitate, whereas

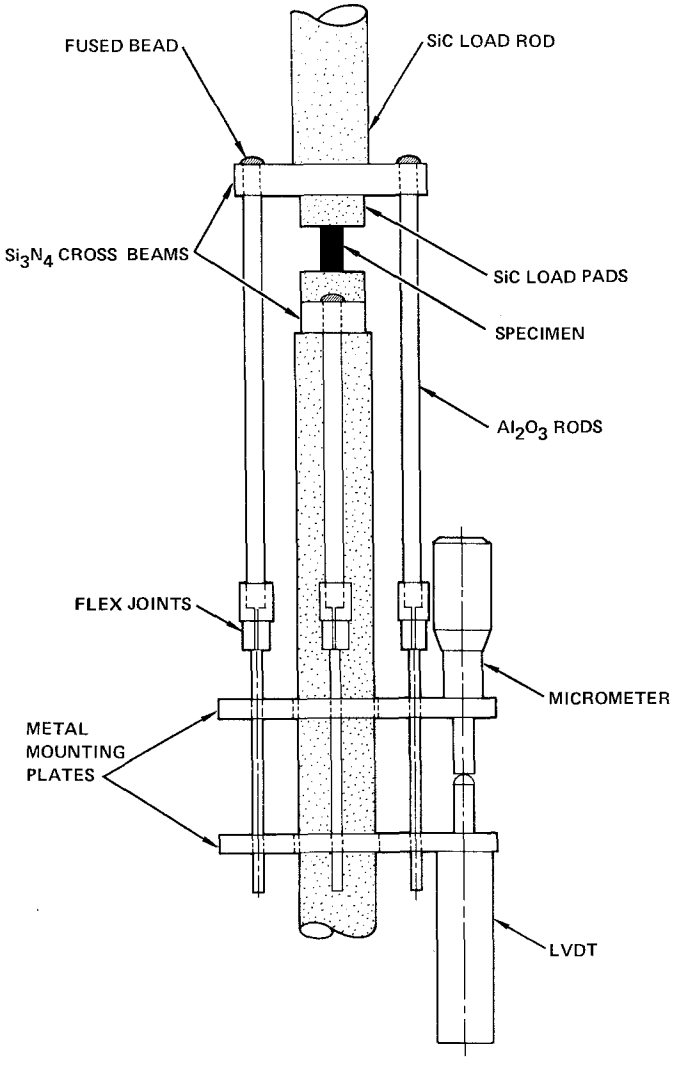

Figure 10 High-temperature extensometer developed for present study.

materials with smaller V_1 do not cavitate and appear to exhibit diffusional creep behaviour (Figs. 4 and 3, respectively) within the stress range examined;

(2) cavitation increases with increasing stress (Fig. 5); the stress dependence appears to mimic that expected for Equation 4;

(3) at lower stresses, the strain rates of all materials are more similar to one another relative to their large divergence at larger stresses, suggesting the dominance of diffusional creep at lower stresses in all materials relative to the dominance of cavitational creep in materials prone to cavitate (B and D) at higher stresses;

(4) tertiary creep behaviour is expected for those materials prone to cavitate as expressed by Equation 4.

It should be noted that at very high stresses, e.g. stress levels that exist at crack fronts, cavitational creep is expected to dominate. Cavitational creep at the crack front will cause sub-critical crack growth by the growth and linking of vapour bubbles [20]. Thus, it can be seen that the compositional dependence of the creep behaviour of Si_3N_4 alloys is of direct concern to their high-temperature fracture behaviour.

Appendix. High-temperature axial extensometer for compressive creep in air

The extensometer used in the high-temperature (1400° C) compressive creep tests is shown schematically in Fig. 10. The silicon carbide load rods are mounted in water-cooled holders outside the furnace. The ends which contact the extensometer are lapped flat and adjusted parallel. The two Si_3N_4 cross beams are identical and oriented at right angles to each other. Silicon carbide load

pads are used between the specimen and cross beams to minimize deformation of the pads and distribute the load into the cross beams. The alumina rods transmit the specimen deformation to the metal mounting plates located below the furnace. Each rod has a flex joint to assist in alignment of the parts. The linear variable differential transducer (LVDT) senses the motion of the mounting plates. The micrometer mounted in the upper metal plate is used to null the transducer output at the start of a creep test. It is also used to calibrate the output of the transducer signal.

Acknowledgement

This work was supported by the Air Force Office of Scientific Research, Contact No. F49620-77-C-0072.

References

1. N. J. OSBORNE, *Proc. Brit. Ceram. Soc.* **25**, *Mech. Prop. of Ceramics* (2) (1975) 263.
2. M. S. SELTZER, *Bull. Am. Ceram. Soc.* **56** (1977) 418.
3. R. KOSSOWSKY, D. G. MILLER and E. S. DIAZ, *J. Mater. Sci.* **10** (1925) 983.
4. S. V. DIN and P. S. NICHOLSON, *ibid.* (1975) 1375.
5. J. M. BIRCH and B. WILSHIRE, *ibid.* **13** (1978) 2627.
6. M. H. LEWIS, B. D. POWELL, P. DREW, R. J. LUMBY, B. NORTH and A. J. TAYLOR, *ibid.* **12** (1977) 61.
7. F. F. LANGE and C. A. ANDERSON, *Bull. Amer. Ceram. Soc.* (in press).
8. J. L. ISKOE, F. F. LANGE and E. S. DIAZ, *J. Mater. Sci.* **11** (1976) 908.
9. D. R. CLARKE and G. THOMAS, *J. Amer. Ceram. Soc.* **60** (1977) 491.
10. L. K. V. LOU, T. E. MITCHELL and A. H. HEUER, *ibid.* **61** (1978) 392.
11. F. F. LANGE, *J. Amer. Ceram. Soc.* (in press).
12. *Idem, ibid.* 64 (1978) 53.
13. *Idem,* Task I: Fabrication, Microstructure and Selected Properties of SiAlON Compositions, Final Rpt. Naval Air Systems Command, Cont. No. N00019-73-C-0208, 16 February (1974).
14. D. R. CLARKE, *Ultramicroscopy* **4** (1979) 33.
15. F. F. LANGE, B. I. DAVIS and D. R. CLARKE, *J. Mater. Sci.* **15** (1980) 616.
16. F. F. LANGE, D. R. CLARKE and B. I. DAVIS, *ibid.* **15** (1980) 611.
17. D. R. CLARKE and F. F. LANGE, (to be published).
18. R. L. STOCKER and M. F. ASHBY, *Rev. Geophys. Space Phys.* **11** (1973) 391.
19. F. F. LANGE, "Non-Elastic Deformation of Polycrystals with a Liquid Boundary Phase", in *Deformation of Ceramic Materials,* edited by R. C. Bradt and R. E. Tressler (Plenum, New York, 1976) pp. 361–81.
20. *Idem, J. Amer. Ceram. Soc.* **62** (1979) 222.

Received 5 July and accepted 28 August 1979.